Note on the bulk estimate of the energy dissipation rate in the bottom boundary layer

XIAOZHOU RUAN*

Department of Earth, Atmospheric, and Planetary Sciences, Massachusetts Institute of Technology, Cambridge, Massachusetts

**Corresponding author address:* Xiaozhou Ruan, Department of Earth, Atmospheric, and Planetary Sciences, Massachusetts Institute of Technology, 77 Massachusetts Ave., Cambridge, MA 02139.

E-mail: xruan@mit.edu

ABSTRACT

The dissipation of the kinetic energy (KE) associated with oceanic flows is believed to occur primarily in the oceanic bottom boundary layer (BBL) where bottom drag converts the KE from mean flows to heat loss through irreversible mixing at molecular scales. Due to the practical difficulties associated with direct observations on small-scale turbulence close to the seafloor, most up-to-date estimates on bottom drag rely on a simple bulk formula ($C_d U^3$) proposed by G.I. Taylor that relates the integrated BBL dissipation rate to a drag coefficient (C_d) as well as a flow magnitude outside of the BBL (U). Using output from several turbulence-resolving Direct Numerical Simulations, it is shown that the true BBL-integrated dissipation rate is about 90% of that estimated using the classic bulk formula, applied here to the simplest scenario where a mean flow is present over a flat and hydrodynamically-smooth bottom. It is further argued that Taylor's formula only provides an upper bound estimate and should be applied with caution in future quantification of BBL dissipation; the performance of the bulk formula depends on the distribution of velocity and shear stress near the bottom, which in the real ocean, could be disrupted by bottom roughness.

1. Introduction

Large-scale ocean currents are primarily powered by atmospheric winds and astronomical tidal forces at rates well quantified through satellite observations (Wunsch and Ferrari 2004). The work done by winds acting on the large-scale ocean currents inputs kinetic energy (KE) at a rate of around 0.8-0.9 TW (Wunsch 1998; Wunsch and Ferrari 2004; Scott and Xu 2009), but the subsequent fate of this KE flux remains elusive. A large fraction of the KE input is converted into a vigorous mesoscale eddy field through baroclinic instabilities of the large-scale currents and accounts for about 90% of the total ocean KE (Ferrari and Wunsch 2009). It is a topic of active research how the mesoscale energy is eventually dissipated at molecular scales. A prime candidate is thought to be bottom drag, i.e. the generation of vigorous turbulence along the ocean seafloor which effectively transfers energy to smaller dissipative scales. Problematically, attempts to estimate the energy dissipated through bottom drag have resulted in widely differing estimates (Wunsch and Ferrari 2004; Sen et al. 2008; Arbic et al. 2009; Wright et al. 2013)

Bottom drag is experienced by oceanic flows above the seafloor where a stress develops that brings the flow to zero. This occurs in a thin bottom boundary layer (BBL) characterized by enhanced shear and turbulence. The bottom stress τ_b is given by:

$$\tau_b \equiv \rho_0 \nu \left.\frac{\partial u}{\partial z}\right|_{z=0}, \tag{1}$$

where ν is the molecular viscosity, ρ_0 is a reference density (seawater density varies by no more than a few percent across the global ocean), $u(z)$ is the velocity component parallel to the seafloor. The bottom friction is often expressed in terms of a friction velocity defined as $u_\tau \equiv \sqrt{\tau_b/\rho_0}$.

In a turbulent flow it is difficult to estimate the bottom stress using formula (1), because it requires detailed knowledge of rapid shear fluctuations very close to the boundary. Instead the bottom stress is typically calculated using an empirical quadratic drag law $\tau_b \simeq \rho_0 C_d U^2$, where

C_d is a drag coefficient and U is the magnitude of the mean flow above the BBL, the so called "far-field" velocity. This formula relates the bottom stress to dynamic pressure (proportional to U^2) associated with the mean flow (Tritton 2012).

Taylor (1920) went a step further and proposed to estimate the KE dissipation within the BBL, $\mathscr{D}$, as the product of the bottom stress and the "far-field" velocity:

$$\mathscr{D} \equiv \int_{\mathrm{BBL}} \varepsilon(z)\, dz \simeq \frac{\tau_b}{\rho_0} U \simeq C_d U^3, \tag{2}$$

where ε is the point-wise KE dissipation rate defined as

$$\varepsilon = \frac{\nu}{2} < S_{ij} S_{ij} >, \tag{3}$$

and $S_{ij} = \partial u_i/\partial x_j + \partial u_j/\partial x_i$ is the rate of strain tensor and the angle bracket denotes a Reynolds average. Taylor (1920) used this bulk formula to estimate the dissipation experienced by barotropic tides over continental shelves and set U to be the barotropic tidal velocity. This bulk formula was later used to estimate dissipation of sub-inertial flows in the global ocean and returned values anywhere between 0.2 and 0.83 TW (Wunsch and Ferrari 2004; Sen et al. 2008; Arbic et al. 2009; Wright et al. 2013). Based on these estimates, bottom drag could be a dominant sink of the 0.8-0.9 TW KE input by winds or a second order process.

In this study, we will take a closer look at the reasoning and assumptions behind Taylor's KE energy dissipation formula (equation (2)). We find that although the formula slightly overestimates the integrated BBL energy dissipation rate, it provides satisfying bulk estimates in idealized numerical simulations of flows over a smooth flat bottom. The difference between the two depends on the distribution of velocity and shear stress close to the seafloor, which implies possibly larger discrepancy when the inner layer structure is disrupted by bottom roughness in the real ocean. The Direct Numerical Simulation (DNS) data are described in section 2. In section 3 we illustrate how the vertical profiles of stress and velocity shear determine the performance of Taylor's formula which is fully recovered only in the limit of infinite Reynolds number. Our hypothesis is confirmed by computing the vertical profiles of shear, stress and KE dissipation from the DNS in section 4. The implications of our work for oceanographic estimates of energy dissipation in the BBL are discussed in section 5.

2. Data and Methods

The data analyzed in this study come from four DNS of a mean flow over a smooth flat bottom, two without rotation (Schlatter and Örlü 2010) and two with rotation (Miyashita et al. 2006), the so called bottom Ekman layer. The simulations are characterized using frictional Reynolds number $\mathrm{Re}_\tau = u_\tau \delta/\nu = \delta/\delta_\nu$, where $\delta_\nu = \nu/u_\tau$ is the viscous length scale. The bottom boundary condition is no-slip in all simulations, and the top boundary condition is a prescribed velocity equal to the free-stream flow. The diagnostics are obtained by horizontally averaging over the model domain once the solutions have achieved a statistically steady state. More details about the simulations are given in Table (1).

For the rest of the paper, we will use δ as the boundary layer thickness for both setups. In the non-rotating case, δ denotes the distance across the boundary layer from the bottom wall to a point where the flow velocity has essentially reached the 'free-stream' velocity (99% of U); in the rotating case, we adopt the common Ekman layer scaling, $\delta = u_\tau/f$, where f is the Coriolis frequency. Considering the difference in the definition of boundary layer thickness, we will use $\mathrm{Re}_\tau = u_\tau\delta/\nu$ for the non-rotating BBL and $\mathrm{Re}_f = u_\tau^2/f\nu$ for the rotating BBL, where the boundary layer thickness is replaced with the Ekman layer scaling. Note, however, that these two Reynolds numbers are comparable as will be shown in section 4. Finally, all the diagnostics are non-dimensionalized by the appropriate combination of frictional variables ν and u_τ; for instance, the non-dimensional dissipation rate is given by $\varepsilon^+ = \varepsilon\nu/u_\tau^4$.

3. The impact of the vertical shear profile on BBL dissipation

We start by computing the integrated BBL dissipation in the non-rotating BBL for idealized vertical shear profiles to illustrate their impact on the bulk estimates. Assuming no horizontal variations in any of the variables, the BBL dissipation is given by,

$$\mathfrak{D} = -\int_0^\delta u \frac{\partial \tau}{\partial z}\, dz = \int_0^\delta \tau \frac{\partial u}{\partial z}\, dz = \int_0^\delta C_D U^2 \left(\frac{\delta - z}{\delta}\right) \frac{\partial u}{\partial z}\, dz. \tag{4}$$

where τ includes both viscous and Reynolds stresses and we integrated by parts using the fact that the velocity u vanishes at $z = 0$ and the stress vanishes at $z = \delta$. The shear stress has been approximated as a linearly decaying profile in z (Pope 2001): $\tau = C_D U^2 \left(\frac{\delta - z}{\delta}\right)$. Taylor's formula follows from equation (4) only if the velocity profile u is uniform and equal to the far-field velocity U, but this is not the case in reality. Instead the velocity profile decays to zero within the BBL due to the no-slip bottom boundary condition. If we assume for simplicity that the velocity profile is linear in z up to $z = \delta_s$, where it reaches the far-field velocity U, and remains constant above (Fig. 1) (in other words, the velocity shear is confined in a thin layer of thickness δ_s near the bottom), the integral in equation (4) can be re-written as:

$$\mathfrak{D} = \int_0^{\delta_s} C_d U^2 \left(\frac{\delta - z}{\delta}\right) \frac{U}{\delta_s}\, dz = C_d U^3 (1 - \frac{1}{2}\frac{\delta_s}{\delta}). \tag{5}$$

For this admittedly idealized piece-wise linear velocity velocity profile, Taylor's formula is recovered only in the limit where the velocity shear is confined to a layer much thinner than the BBL ($\delta_s \ll \delta$).

The vertical profiles of velocity in the non-rotating BBL are shown in Fig. 2a for two different Re_τ. As Re_τ increases, the layer accounting for the velocity shear becomes thinner and closer to the wall. While the shear layer thickness is always thinner than δ, and progressively more so for increasing Re_τ, it clearly differs from the limit where the shear layer is infinitesimally thin as assumed in Taylor's formula. We will evaluate the impact of this discrepancy in the next section.

4. Vertical structures of the BBL

a. Non-rotating BBL

Along with the thin layer containing the large velocity shear is enhanced viscous stress and the associated dissipation of mean kinetic energy (MKE) within the BBL (Fig. 2b, c). The viscous stress is dominant for $z/\delta < 0.1$ due to both the enhanced velocity shear and the damping of Reynolds stress in the presence of the solid bottom. The distribution of the total shear stress provides support for the linear approximation made in the idealized heuristic model in the last section. As Re_τ increases, both the viscous and Reynolds stress become closer to the bottom, but the structure of the total shear stress remains relatively unchanged (Fig. 2b).

The dissipation of MKE acts as an additional route to energy dissipation and has been typically thought to be negligible in turbulent flows away from boundaries with moderate to large Reynolds numbers. It cannot be ignored, however, in the BBL where the velocity shear is confined close to the bottom. In this case, MKE dissipation contributes around 40% of the total energy dissipation rate. As expected, the dissipation of MKE is active to at least $z/\delta = 0.1$ where the dissipation rate drops by two orders of magnitude from the bottom value, consistent with the distribution of viscous stress. On the other hand, the dissipation of turbulent kinetic energy (TKE) becomes dominant starting below $z/\delta = 0.1$ and remains so all the way to the top of the BBL. The transition point between the dissipation of MKE and TKE becomes closer to the bottom with larger Re_τ.

In these two simulations of non-rotating BBL, the true integrated KE dissipation rate is 86.1% and 86.4% of those estimated using Taylor's bulk formula (Table 1), implying that the δ_s/δ ratio in equation (5) is about 0.28; this depth of shear layer δ_s roughly corresponds to $\varepsilon^+ = 10^{-4}$ (Fig. 2c). We will examine the performance of Taylor's formula in the rotating BBL next.

b. Rotating BBL

When rotation is introduced, the velocity profiles show a spiral structure as they approach the far-field mean flow (Fig. 3a). One noticeable difference from the non-rotating BBL is more bottom-confined, or concave profiles for both velocity shear and shear stress (Fig. 3a, b), compared with the more linear shear profile in the non-rotating BBL. The rest structures remain similar in the BBL with or without rotation.

In the two simulations of rotating BBL, the true integrated KE dissipation rate is 90.8% and 91.8% of those estimated using Taylor's bulk formula, higher than those for the non-rotating BBL for comparable Re_f. With a similar δ_s/δ ratio, this better performance could be explained by the more bottom-confined velocity shear the shear stress profiles.

In summary, Taylor's bulk formula provides reasonable first-order estimates for the true integrated dissipation rate. In fact, $\mathscr{D}/C_d U^3 \approx 0.9$ which is equivalent of a $\delta_s/\delta \approx 0.2$ is consistent with the observations that the log-layer, where the largest velocity shear and shear stress reside, roughly occupies 20% of the BBL thickness for both the rotating and non-rotating BBLs (Fig. 4). This 20% has also been shown to hold for natural turbulent flows with much larger Re_τ (Marusic et al. 2013), which implies that Taylor's formula could provide a reasonable integrated dissipation estimate in the real ocean, given that the log-layer structure remains intact.

5. Conclusions and discussions

Four DNS experiments were used to demonstrate that the dissipation of kinetic energy in the bottom boundary layer (BBL) over a flat wall is less than predicted by the celebrated formula proposed by Taylor (1920): $\mathscr{D} \simeq C_D U^3$, where C_D is a constant drag coefficient and U the 'far-field' velocity above the BBL. Taylor's estimate should be treated as an upper and singular limit of the true BBL-integrated KE dissipation rate. The discrepancy arises due to the assumption that the shear in the BBL is confined to an infinitesimally thin layer within the viscous sublayer in Taylor's formula. It is shown that the shear actually extends way above the viscous sublayer to about 20% of the BBL thickness for even the largest frictional Reynolds numbers Re_τ expected in natural flows and this results in a smaller energy dissipation rate. Taylor's formula could thus be improved to be: $\mathscr{D} \approx 0.9 \times C_D U^3$ in these cases.

Admittedly, Taylor's formula provides a good first-order estimate for the integrated BBL dissipation rate. However, the evaluation performed in this note only applies to smooth bottom where the viscous and log-layers are intact. The ocean seafloor is far from flat. Corrugations on scales smaller than the BBL thickness, typical of the ocean seafloor could modify or even destroy the inner layer structures (Jiménez 2004). The small roughness can be accounted for by introducing a roughness parameter which quantifies the characteristic height of the corrugations, z_o. This results in a modification of the log-layer away from the bottom: $u(z) = \frac{u_\tau}{\kappa} \log \frac{z}{z_o}$ (e.g. Pope 2001; Tennekes and Lumley 2018). It remains to be studied whether the disrupted viscous sublayer and the modified log-layer structure could have an impact on the energy dissipation estimate. Moreover, the log-layer could be completely destroyed when the roughness is large. A common parameter to consider here is the blockage ratio δ/k where k is the roughness height. This non-dimensional parameter measures the direct effect of the roughness on the log-layer, where most of the mean shear are concentrated. Previous studies have shown that δ/k has to be at least 40 for a general log-layer structure to hold (Jiménez 2004). This suggests that Taylor's formula could fail over rough seafloors where the velocity shear is no longer concentrated close to the wall.

The DNS experiments presented here do not include stratification. This may not be the most problematic simplification of our work, because stratification is expected to be quite weak in oceanic BBL. Stratification is indeed very weak in the inner layer close to the seafloor due to enhanced mixing (e.g. Perlin et al. 2007; Ruan et al. 2017). Stratification may however be strong enough in the outer layer to suppress turbulent overturns larger than the Ozmidov scale $L_o = (\varepsilon/N^3)^{1/2}$ (N being the Brunt-Väisälä frequency) and lead to a modification of the shear profile (Sanford and Lien 1999; Perlin et al. 2005). However we showed that the bulk of the KE dissipation occurs in the log-layer, and not in the outer layer, where the distance to the bottom is the dominant limit on the eddy overturn size rather than the Ozimdov scale. Thus, we expect the influence of stratification on the integrated dissipation rate to be small.

In addition to small-scale roughness, BBL dissipation can be modified by the presence of large-scale slopes, like along the flanks of ridges and seamounts (Callies 2018; Wenegrat et al. 2018; Ruan and Callies 2020), detachment of BBL at large Froude numbers (e.g. Armi 1978), and development of a whole gamut of hydrodynamic subemsoscale instabilities, hydraulic jumps (e.g. Thurnherr et al. 2005; Wenegrat and Thomas 2020). Clearly a full quantitative picture of BBL dissipation in the ocean remains far from complete. Our work has only shown that Taylor's formula should be used with caution and treated as an upper limit of the integrated BBL dissipation rate in the case of a mean flow over the seafloor. Future examinations are needed to account for seafloor roughness and more realistic velocity and stress profiles before applying Taylor's formula in global energy dissipation studies.

Acknowledgments. I thank Raffaele Ferrari for helpful discussions and comments that improved the manuscript.

References

Arbic, B. K., and Coauthors, 2009: Estimates of bottom flows and bottom boundary layer dissipation of the oceanic general circulation from global high-resolution models. *Journal of Geophysical Research: Oceans*, **114 (C2)**.

Armi, L., 1978: Some evidence for boundary mixing in the deep ocean. *Journal of Geophysical Research: Oceans*, **83 (C4)**, 1971–1979.

Callies, J., 2018: Restratification of abyssal mixing layers by submesoscale baroclinic eddies. *Journal of Physical Oceanography*, **48 (9)**, 1995–2010.

Ferrari, R., and C. Wunsch, 2009: Ocean circulation kinetic energy: Reservoirs, sources, and sinks. *Annual Review of Fluid Mechanics*, **41**.

Jiménez, J., 2004: Turbulent flows over rough walls. *Annu. Rev. Fluid Mech.*, **36**, 173–196.

Marusic, I., J. P. Monty, M. Hultmark, and A. J. Smits, 2013: On the logarithmic region in wall turbulence. *Journal of Fluid Mechanics*, **716**.

Miyashita, K., K. Iwamoto, and H. Kawamura, 2006: Direct numerical simulation of the neutrally stratified turbulent ekman boundary layer. *Journal of the Earth Simulator*, **6**, 3–15.

Perlin, A., J. Moum, J. Klymak, M. Levine, T. Boyd, and P. Kosro, 2007: Organization of stratification, turbulence, and veering in bottom ekman layers. *Journal of Geophysical Research: Oceans*, **112 (C5)**.

Perlin, A., J. N. Moum, J. Klymak, M. D. Levine, T. Boyd, and P. M. Kosro, 2005: A modified law-of-the-wall applied to oceanic bottom boundary layers. *Journal of Geophysical Research: Oceans*, **110 (C10)**.

Pope, S. B., 2001: Turbulent flows. IOP Publishing.

Ruan, X., and J. Callies, 2020: Mixing-driven mean flows and submesoscale eddies over mid-ocean ridge flanks and fracture zone canyons. *Journal of Physical Oceanography*, **50 (1)**, 175–195.

Ruan, X., A. F. Thompson, M. M. Flexas, and J. Sprintall, 2017: Contribution of topographically generated submesoscale turbulence to Southern Ocean overturning. *Nature Geoscience*, **10 (11)**, 840.

Sanford, T. B., and R.-C. Lien, 1999: Turbulent properties in a homogeneous tidal bottom boundary layer. *Journal of Geophysical Research: Oceans*, **104 (C1)**, 1245–1257.

Schlatter, P., and R. Örlü, 2010: Assessment of direct numerical simulation data of turbulent boundary layers. *Journal of Fluid Mechanics*, **659**, 116–126.

Scott, R. B., and Y. Xu, 2009: An update on the wind power input to the surface geostrophic flow of the world ocean. *Deep Sea Research Part I: Oceanographic Research Papers*, **56 (3)**, 295–304.

Sen, A., R. B. Scott, and B. K. Arbic, 2008: Global energy dissipation rate of deep-ocean low-frequency flows by quadratic bottom boundary layer drag: Computations from current-meter data. *Geophysical Research Letters*, **35 (9)**.

Taylor, G. I., 1920: I. tidal friction in the irish sea. *Philosophical Transactions of the Royal Society of London. Series A, Containing Papers of a Mathematical or Physical Character*, **220 (571-581)**, 1–33.

Tennekes, H., and J. L. Lumley, 2018: *A first course in turbulence*. MIT press.

Thurnherr, A., L. St. Laurent, K. Speer, J. Toole, and J. Ledwell, 2005: Mixing associated with sills in a canyon on the midocean ridge flank. *Journal of physical oceanography*, **35 (8)**, 1370–1381.

Tritton, D. J., 2012: *Physical fluid dynamics*. Springer Science & Business Media.

Wenegrat, J. O., J. Callies, and L. N. Thomas, 2018: Submesoscale baroclinic instability in the bottom boundary layer. *Journal of Physical Oceanography*, **48 (11)**, 2571–2592.

Wenegrat, J. O., and L. N. Thomas, 2020: Centrifugal and symmetric instability during ekman adjustment of the bottom boundary layer. *Journal of Physical Oceanography*, **50 (6)**, 1793–1812.

Wright, C. J., R. B. Scott, D. Furnival, P. Ailliot, and F. Vermet, 2013: Global observations of ocean-bottom subinertial current dissipation. *Journal of Physical Oceanography*, **43 (2)**, 402–417.

Wunsch, C., 1998: The work done by the wind on the oceanic general circulation. *Journal of Physical Oceanography*, **28 (11)**, 2332–2340.

Wunsch, C., and R. Ferrari, 2004: Vertical mixing, energy, and the general circulation of the oceans. *Annu. Rev. Fluid Mech.*, **36**, 281–314.

LIST OF TABLES

TABLE 1. Summary of the DNS experiments

No.	$\mathrm{Re}_\tau(\mathrm{Re}_f)$	u_τ/U	Type	$\mathscr{D}/C_d U^3$
1	830	4.08×10^{-2}	non-rotating	0.8614
2	1271	3.85×10^{-2}	non-rotating	0.8638
3	943	5.61×10^{-2}	rotating	0.9082
4	1765	5.21×10^{-2}	rotating	0.9178

LIST OF FIGURES

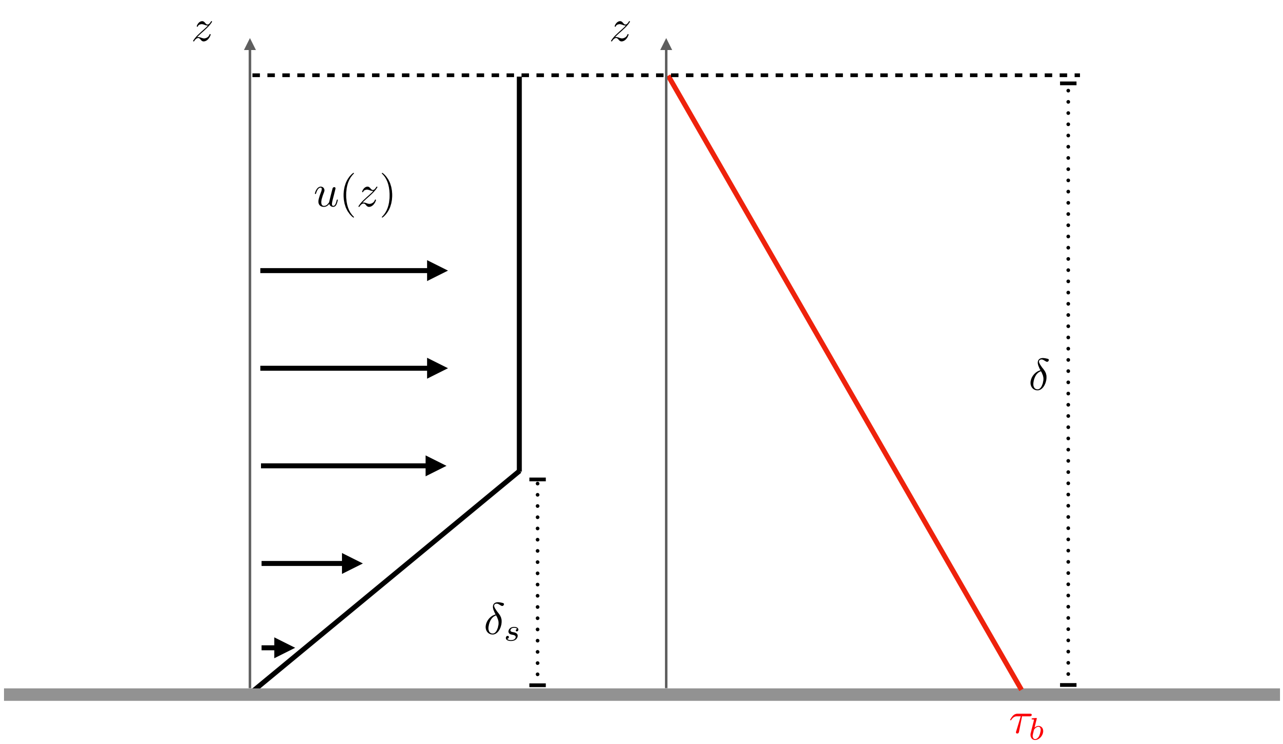

271 FIG. 1. Schematic of idealized distribution of velocity and shear stress in the non-rotating bottom boundary layer (BBL). On the left is the mean velocity profile as a function of depth where a constant shear layer of thickness δ_s is present. On the right is the linearly decaying profile of shear stress where it takes the bottom stress value $\tau = \tau_b$ at $z = 0$ and $\tau = 0$ at $z = \delta$.

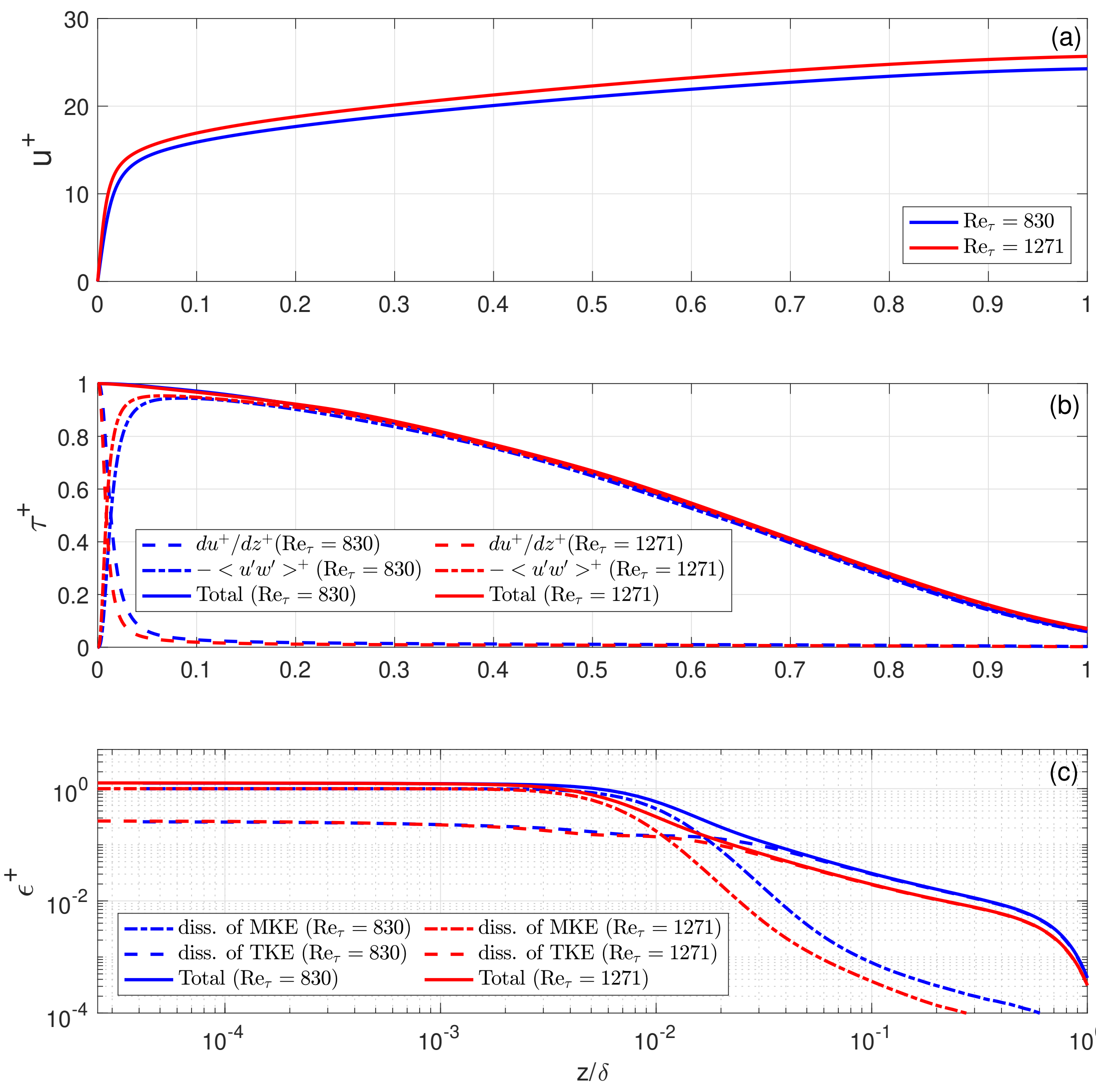

FIG. 2. Profiles of nondimensional velocity (a), shear stress (b) and dissipation rate (c) as a function of z/δ (depth normalized by the boundary layer thickness) in the non-rotating BBL.

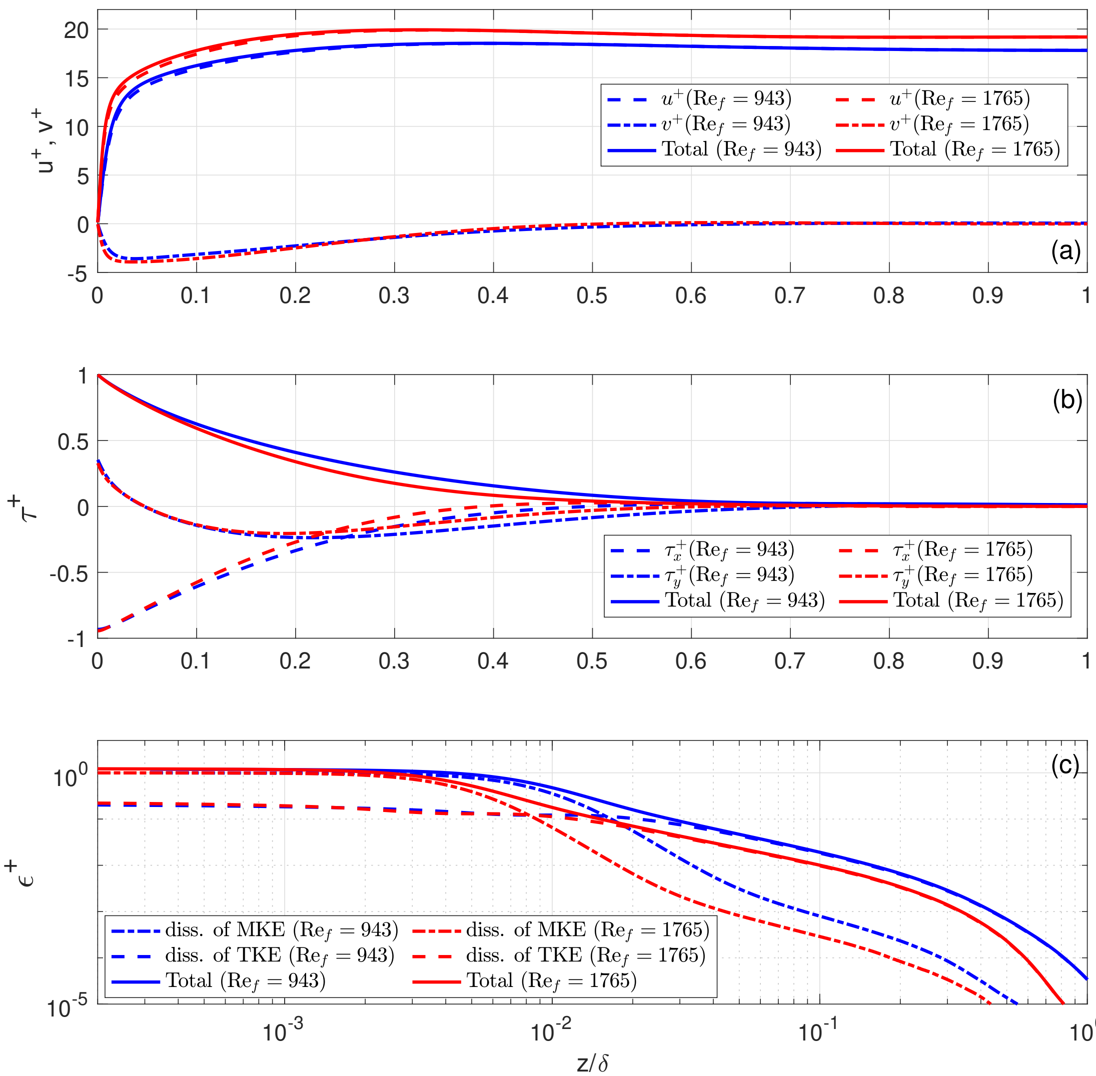

FIG. 3. Profiles of nondimensional velocity (a), shear stress (b) and dissipation rate (c) as a function of z/δ (depth normalized by the boundary layer thickness) in the rotating BBL.

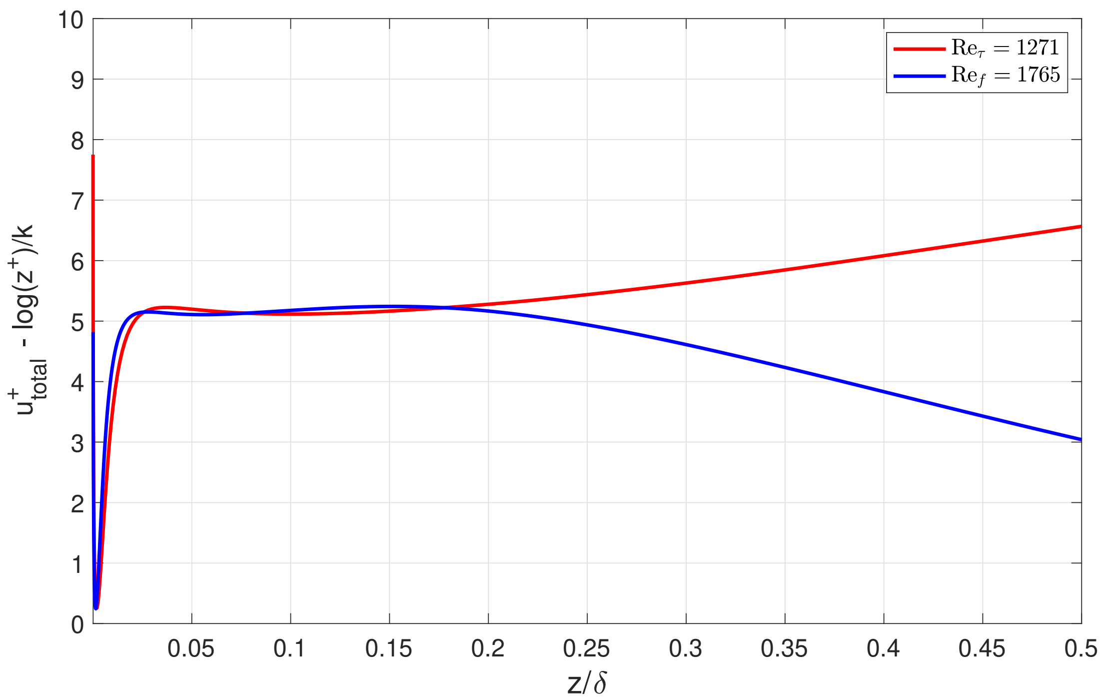

FIG. 4. The difference between nondimensional velocity and a logarithmic function of depth (z^+) where the flat lines indicate the logarithmic layer. Both the rotating and non-rotating profiles are shown here.